

# Controlling Bulk Conductivity in Topological Insulators: Key Role of Anti-Site Defects

D. O. Scanlon,\* P. D. C. King,\* R. P. Singh, A. de la Torre, S. McKeown Walker, G. Balakrishnan, F. Baumberger, and C. R. A. Catlow

The binary Bi-chalcogenides,  $\text{Bi}_2\text{Ch}_3$ , are widely regarded as model examples of a recently discovered new form of quantum matter, the three-dimensional topological insulator (TI).<sup>[1–4]</sup> These compounds host a single spin-helical surface state which is guaranteed to be metallic due to time reversal symmetry, and should be ideal materials with which to realize spintronic and quantum computing applications of TIs.<sup>[5]</sup> However, the vast majority of such compounds synthesized to date are not insulators at all, but rather have detrimental metallic bulk conductivity.<sup>[2,3]</sup> This is generally accepted to result from unintentional doping by defects, although the nature of the defects responsible across different compounds, as well as strategies to minimize their detrimental role, are surprisingly poorly understood. Here, we present a comprehensive survey of the defect landscape of Bi-chalcogenide TIs from first-principles calculations. We find that fundamental differences in the energetics of native defect formation in Te- and Se-containing TIs enables precise control of the conductivity across the ternary Bi-Te-Se alloy system. From a systematic angle-resolved photoemission (ARPES) investigation of such ternary alloys, combined with bulk transport measurements, we demonstrate that this method can be utilized to achieve intrinsic topological insulators with only a single Dirac cone surface state intersecting the chemical potential. Our microscopic calculations reveal the key role of anti-site defects for achieving this, and predict optimal growth conditions to realize maximally-resistive ternary TIs.

**Figure 1** shows the calculated Fermi-level-dependent formation energies of native defects in the binary TIs  $\text{Bi}_2\text{Se}_3$  and  $\text{Bi}_2\text{Te}_3$ . For  $\text{Bi}_2\text{Se}_3$  under Bi-rich/Se-poor conditions (Figure 1a), Se vacancies in the two inequivalent chalcogen layers,  $V_{\text{Se}}^1$  and

$V_{\text{Se}}^2$ , are the dominant donor defects. In particular,  $V_{\text{Se}}^1$  has the lowest formation energy of all of the native defects for Fermi levels across the entire bulk bandgap, and even up in to the conduction band. This will result in a strong propensity for the formation of *n*-type defects, without significant compensation from *p*-type defects for bulk Fermi levels up to at least 0.1 eV above the conduction band minimum (CBM). This is entirely consistent with our experimental measurements shown in **Figure 2**. Our ARPES measurements of  $\text{Bi}_2\text{Se}_3$  (Figure 2a), which probe its occupied electronic structure, show not only the bulk valence bands and the topological surface state, but also occupied bulk conduction band states. The Fermi level is located a little over 0.1 eV above the CBM, as expected from our calculations. This results in a large *n*-type conductivity, and a temperature-dependent resistivity (Figure 2b) characteristic of a metal rather than an insulator.

For comparison, we also calculate the formation energies for native defects in  $\text{Bi}_2\text{Se}_3$  under Bi-poor/Se-rich conditions (Figure 1b). Compared to the defect energetics under Bi-rich conditions, one would naively expect the formation energy of  $V_{\text{Se}}$  to increase, while that of the acceptor-type Bi-vacancy to decrease, and this is indeed seen in our calculations. On this basis alone, much lower residual *n*-type conductivities could be expected under Bi-poor growth conditions, with the Fermi level moving into the bulk bandgap (tending towards the intersections of the formation energies of  $V_{\text{Se}}^1$  and  $V_{\text{Bi}}$ ). We find, however, that the donor-type Se anti-site defect,  $\text{Se}_{\text{Bi}}$ , becomes the lowest energy defect throughout the bandgap. Therefore, as well as the commonly assumed  $V_{\text{Se}}$ , our calculations indicate that  $\text{Se}_{\text{Bi}}$  can play a significant role in driving the unintentional conductivity of  $\text{Bi}_2\text{Se}_3$ . For all possible growth conditions, the lowest energy defect is a donor (either  $V_{\text{Se}}^1$  or  $\text{Se}_{\text{Bi}}$ ), even when the Fermi level lies at, or slightly above, the CBM. This explains why crystals of  $\text{Bi}_2\text{Se}_3$  always display unintentional *n*-type conductivity, which can only be compensated by suitable extrinsic *p*-type doping.<sup>[6]</sup>

The defect physics of  $\text{Bi}_2\text{Te}_3$  is rather different, with anti-sites being the dominant defects under both Bi-rich/Te-poor and Bi-poor/Te-rich conditions (Figure 1c,d). Under Bi-poor conditions (Figure 1d), the  $\text{Te}_{\text{Bi}}$  donor defect has the lowest formation energy of all of the native defects. As for  $\text{Bi}_2\text{Se}_3$  under Bi-poor conditions, this will yield unintentional *n*-type conductivity as often observed in experiment,<sup>[3]</sup> with significant compensation by acceptor  $V_{\text{Bi}}$  centres not expected for Fermi levels within the bulk bandgap. However, under Bi-rich conditions the formation energy of the acceptor Bi anti-site defect,  $\text{Bi}_{\text{Te}}^1$ , becomes smaller than that of the chalcogen vacancy (Figure 1c). This is in stark contrast to  $\text{Bi}_2\text{Se}_3$ . It promotes a natural tendency for

Dr. D. O. Scanlon, Prof. C. R. A. Catlow  
University College London  
Kathleen Lonsdale Materials Chemistry  
Department of Chemistry  
20 Gordon Street, London WC1H 0AJ, UK  
E-mail: d.scanlon@ucl.ac.uk

Dr. P. D. C. King, A. de la Torre, S. McKeown Walker,  
Dr. F. Baumberger  
SUPA, School of Physics and Astronomy  
University of St. Andrews  
St. Andrews, Fife KY16 9SS, UK  
E-mail: philip.d.c.king@physics.org  
Dr. R. P. Singh, Dr. G. Balakrishnan  
Department of Physics  
University of Warwick  
Coventry CV4 7AL, UK



DOI: 10.1002/adma.201200187

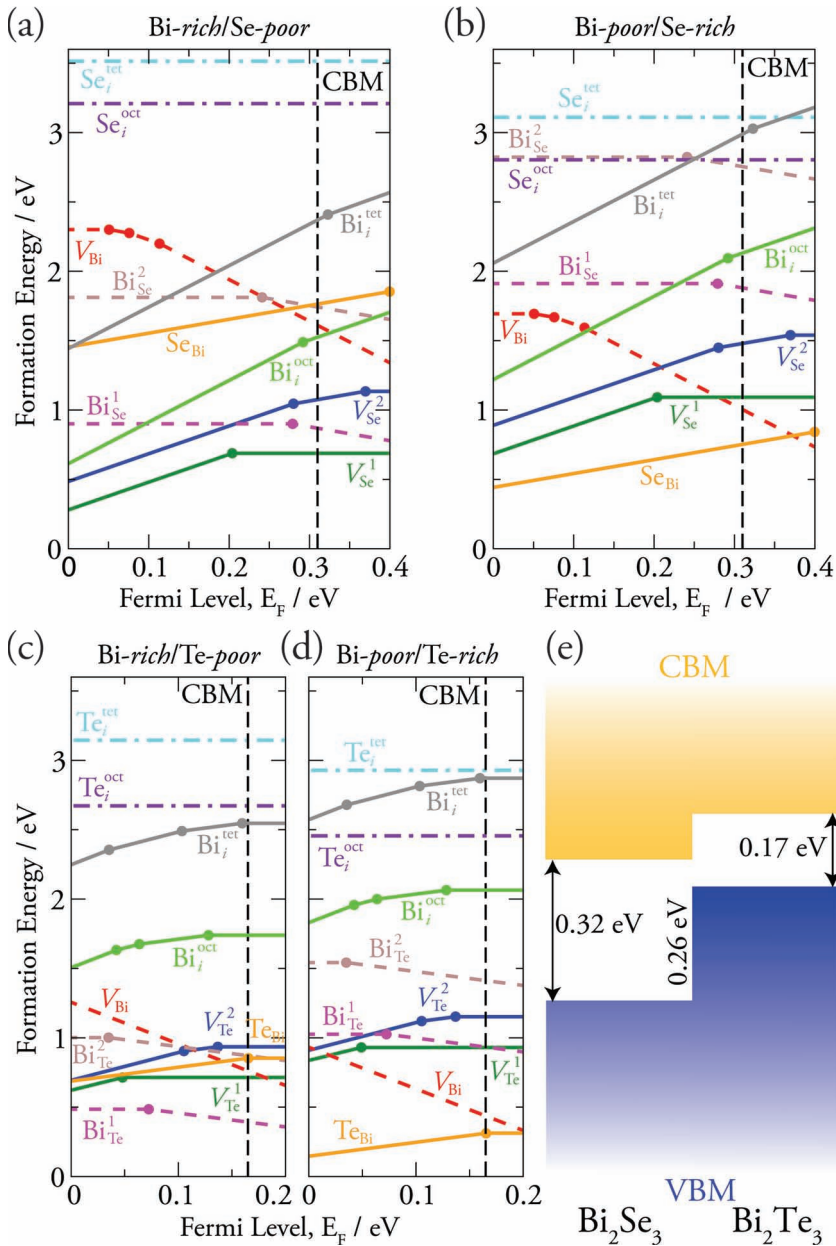


**Figure 1.** Formation energies, as a function of Fermi level relative to the VBM, of donor (solid lines), acceptor (dashed lines) and electrically-inactive (dot-dashed lines) defects in  $\text{Bi}_2\text{Se}_3$  under (a) Bi-rich and (b) Bi-poor conditions. (c,d) Equivalent calculations for  $\text{Bi}_2\text{Te}_3$ . (e) Calculated valence band offset and resulting band alignment of  $\text{Bi}_2\text{Se}_3$  and  $\text{Bi}_2\text{Te}_3$ .

unintentional *p*-type conduction when  $\text{Bi}_2\text{Te}_3$  is grown under Bi-rich conditions, consistent with both single-crystal growth experiments,<sup>[7]</sup> as well as recent studies on MBE-grown thin films.<sup>[8]</sup> Thus, our calculations reveal that the defect landscape of  $\text{Bi}_2\text{Te}_3$  is dominated by anti-site defects for all growth conditions, and anion vacancies play a much less significant role than in  $\text{Bi}_2\text{Se}_3$ .

In fact, as shown in **Table 1**, the energy cost of anti-site disorder in  $\text{Bi}_2\text{Te}_3$  is approximately half that of  $\text{Bi}_2\text{Se}_3$ . This is due to the more similar ionic radii of Bi and Te,<sup>[9]</sup> and the relatively small differences in electronegativity between the two species:

the resulting anti-site defects represent a relatively low-energy configuration. We note that these anti-sites serve to oppose the “expected” polarity of the materials, yielding *p*-type conduction under typical *n*-type growth conditions, and *n*-type samples under typical *p*-type conditions. While growth conditions between these two extremes can yield defect energetics which drive the Fermi level into the bulk bandgap, the small size of this energy gap will make achieving robust insulating behavior very difficult for this compound.

The qualitative differences in the native defect behavior of  $\text{Bi}_2\text{Se}_3$  and  $\text{Bi}_2\text{Te}_3$  can be understood from their band alignment. We have computed the natural valence band offsets of these materials using the methodology of Zunger and co-workers.<sup>[10,11]</sup> We find a staggered “type II” offset (Figure 1e),<sup>[12]</sup> with the valence band maximum (VBM) of  $\text{Bi}_2\text{Te}_3$  0.26 eV higher in energy than that of  $\text{Bi}_2\text{Se}_3$ . The smaller ionization potential of  $\text{Bi}_2\text{Te}_3$  suggests an increased preference for hole formation,<sup>[13]</sup> which fully supports our microscopic calculations. The CBM of  $\text{Bi}_2\text{Se}_3$ , on the other hand, is only 0.10 eV below that of  $\text{Bi}_2\text{Te}_3$ , explaining why both materials display similar *n*-type behavior under Bi-poor growth conditions.

Within a conventional semiconductor band engineering methodology, this suggests that alloying  $\text{Bi}_2\text{Se}_3$  and  $\text{Bi}_2\text{Te}_3$  could be a suitable way to realize bulk insulators, where the topological surface state conduction is no longer shunted by a large residual bulk conductivity. Indeed, transport measurements of the ternary compound  $\text{Bi}_2\text{Te}_2\text{Se}$  have already found a much more insulating bulk resistivity than for the binary compounds,<sup>[14]</sup> although previous ARPES measurements still showed the occupation of a small number of states at the bottom of the conduction band.<sup>[15]</sup> In contrast, our APRES measurements (Figure 2a) show that, upon moving towards Te-rich Bi-Te-Se alloys, the conduction band is readily depleted of carriers.<sup>[16]</sup> In particular, for both  $\text{Bi}_2\text{Te}_2\text{Se}$  and  $\text{Bi}_2\text{Te}_{2.5}\text{Se}_{0.5}$ , only the topological surface state intersects the chemical potential, as desired for a TI.<sup>[18]</sup> Both of these compounds exhibit a temperature dependence of their resistivity indicative of bulk insulators. For  $\text{Bi}_2\text{Te}_2\text{Se}$  (Figure 2b), the low-temperature resistivity is as much as two-to-three orders of magnitude higher than in  $\text{Bi}_2\text{Se}_3$ . However,  $\text{Bi}_2\text{Te}_{2.5}\text{Se}_{0.5}$  has a low-temperature resistivity approximately a factor of 6 lower than  $\text{Bi}_2\text{Te}_2\text{Se}$  (Figure 2b), due to its smaller bandgap.

Thus,  $\text{Bi}_2\text{Te}_2\text{Se}$  can be seen as a more ideal TI, and we perform explicit calculations for this compound in order to elucidate the microscopic origin of its enhanced resistivity as compared to the binary compounds. Both the Te and Se

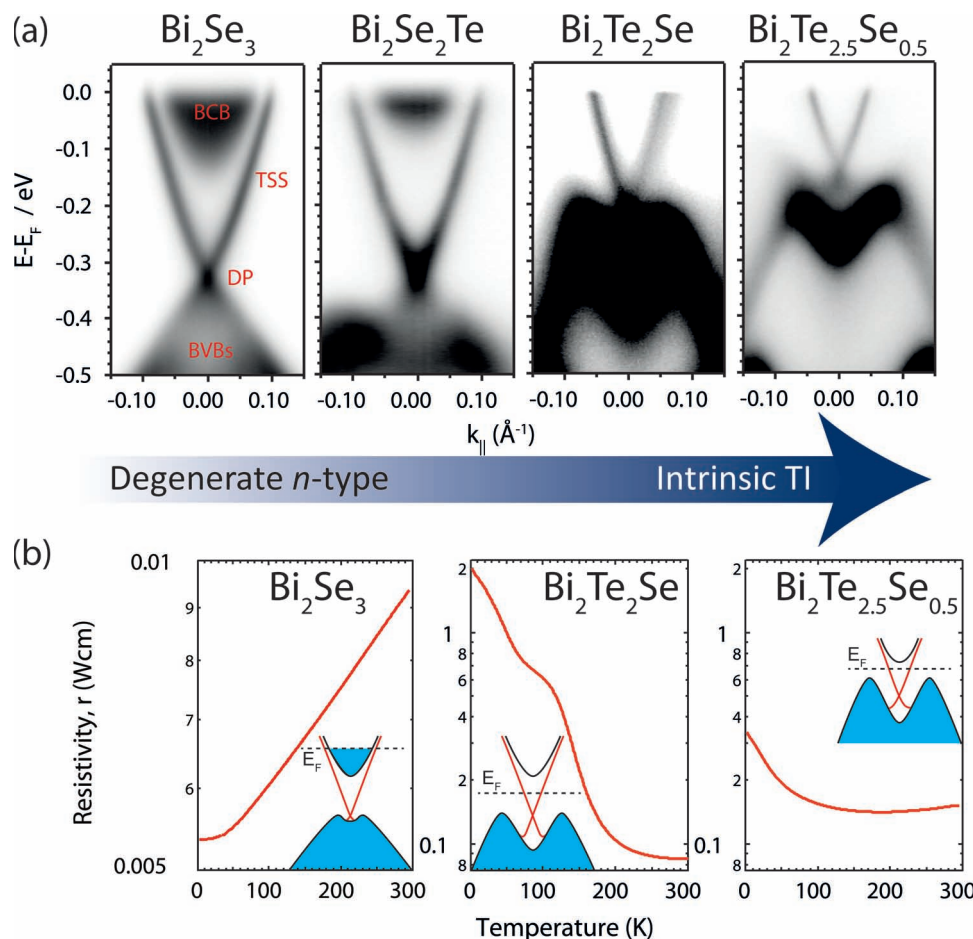


**Figure 2.** (a) ARPES measurements of layered Bi-chalcogenides. The bulk valence bands (BVBs) and topological surface state (TSS) are clearly observed for all compounds. Occupied bulk conduction band (BCB) states are only observed for  $\text{Bi}_2\text{Se}_3$  and  $\text{Bi}_2\text{Se}_2\text{Te}$ , indicating a transition from degenerately doped semiconductors to intrinsic bulk TIs as the Te content is increased. Temperature-dependent resistivity measurements (b) confirm this trend, showing metallic and insulating behaviour for  $\text{Bi}_2\text{Se}_3$ , and  $\text{Bi}_2\text{Te}_2\text{Se}$  and  $\text{Bi}_2\text{Te}_{2.5}\text{Se}_{0.5}$ , respectively. The insets show schematic representations of the electronic structure, with the Fermi level located in the conduction band for  $\text{Bi}_2\text{Se}_3$  and within the bulk bandgap for  $\text{Bi}_2\text{Te}_2\text{Se}$  and  $\text{Bi}_2\text{Te}_{2.5}\text{Se}_{0.5}$ .

chemical potentials can be simultaneously varied, subject to the constraints that  $\text{Bi}_2\text{Te}_2\text{Se}$  has lower formation enthalpy than binary compounds of Bi and Te/Se, or than elemental Bi, Te, or Se. Considering these limits, we follow the approach of Walsh et al.<sup>[20]</sup> and Persson et al.<sup>[21]</sup> to calculate a phase diagram for growth of  $\text{Bi}_2\text{Te}_2\text{Se}$ , shown in **Figure 3a**. We consider five representative environments in which to calculate formation energies of native defects, shown in **Figure 3b**.

**Table 1.** Anti-site disorder energies,  $\Delta E_{ad} = 1/2[E_{A_B} + E_{B_A} - 2E^{\text{pure}}]$ , where  $E_{A_B}$  is the total energy of a supercell containing an  $A_B$  defect, and  $E^{\text{pure}}$  is the energy of the stoichiometric  $\text{Bi}_2\text{Ch}_2\text{Ch}$  supercell.

System	Species involved	$\Delta E/\text{eV}$
$\text{Bi}_2\text{Se}_3$	Bi, Se	1.37
$\text{Bi}_2\text{Te}_3$	Bi, Te	0.67
$\text{Bi}_2\text{Te}_2\text{Se}$	Bi, Se	1.52
	Bi, Te	0.80
	Se, Te	0.13

In addition to the defects considered for the binary compounds, it is now possible to have anion-on-anion anti-site defects ( $\text{Se}_{\text{Te}}$  and  $\text{Te}_{\text{Se}}$ ). In fact, we find that these centers have the lowest formation energy of all native defects across the entire phase diagram. While they have no transition levels within the bandgap, and so are electrically inactive, the energy barrier for anion-on-anion anti-site disorder is as low as only 0.13 eV (Table 1). It therefore seems inevitable that there will be a significant level of anti-site disorder in these compounds. Indeed, previous structural refinements have revealed between approximately 10%,<sup>[25]</sup> and 30%,<sup>[26]</sup> deviation from the nominal ordered anion site occupancy in  $\text{Bi}_2\text{Te}_2\text{Se}$ , entirely consistent with the results of our microscopic calculations.

Depending on the growth environment, the lowest energy *p*-type defects are the Bi vacancy or the  $\text{Bi}_{\text{Te}}$  anti-site, with the dominant *n*-type defects being the Te vacancy or the  $\text{Te}_{\text{Bi}}$  anti-site. Se vacancies and anion-on-cation anti-sites invariably have higher formation energy than their Te counterparts. In all cases, the formation energy of the dominant donor and acceptor defects cross over within the bandgap. Under equilibrium conditions, the Fermi level will tend to be pinned close to

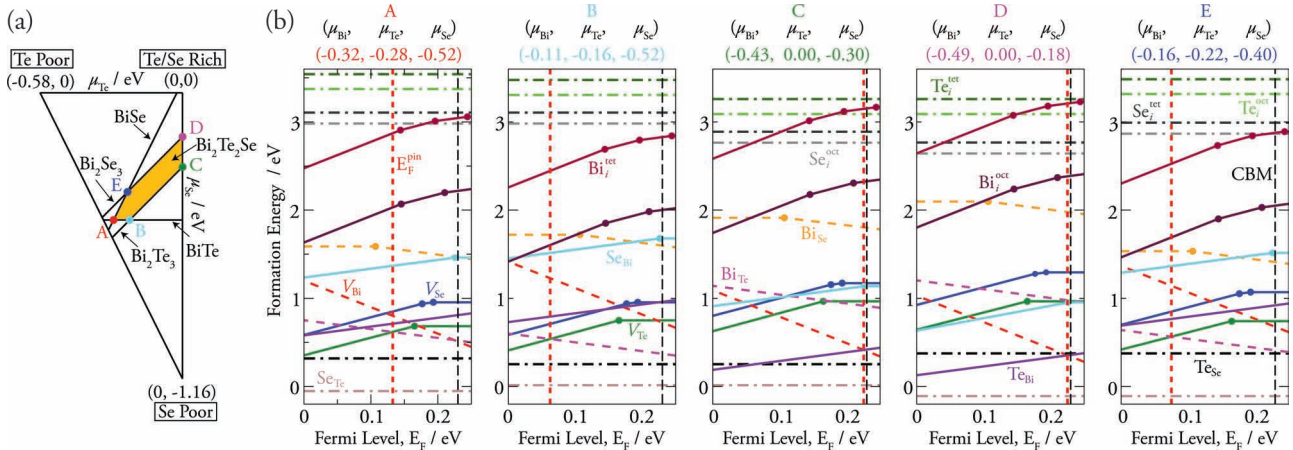


**Figure 3.** (a) Calculated phase diagram of  $\text{Bi}_2\text{Te}_2\text{Se}$  as a function of Te and Se chemical potential. (b) Formation energies for defects in  $\text{Bi}_2\text{Te}_2\text{Se}$ , computed for the five sets of chemical potentials shown in (a).

this crossing point, represented by the vertical red dotted lines in Figure 3b. For Te/Se-rich conditions (C and D in Figure 3b), this is very close to the CBM, and so the bulk conductivity will likely still be rather high. However, for Te- and Se-poor growth conditions (A, B, and E in Figure 3b with  $(\mu_{\text{Bi}}, \mu_{\text{Te}}, \mu_{\text{Se}}) = (-0.32 \text{ eV}; -0.28 \text{ eV}; -0.52 \text{ eV})$ ,  $(-0.11 \text{ eV}; -0.16 \text{ eV}; -0.52 \text{ eV})$ , and  $(-0.16 \text{ eV}; -0.22 \text{ eV}; -0.4 \text{ eV})$ , respectively), this level lies close to the middle of the bandgap, where the formation energy for the doubly-charged donor  $V_{\text{Te}}$  crosses that of the singly-charged acceptor  $\text{Bi}_{\text{Te}}$ . Only considering vacancies, the effective Fermi level pinning would be shifted towards much more *n*-type conditions, and so it is again clear that anti-site defects play a key role controlling the unintentional bulk conductivity of ternary, as well as binary, topological insulators. Scanning tunneling microscopy has already shown evidence for the presence of the anti-site  $\text{Bi}_{\text{Te}}$  defect in binary  $\text{Bi}_2\text{Te}_3$ <sup>[8]</sup>: we hope that similar local-probe measurements of  $\text{Bi}_2\text{Te}_2\text{Se}$  will provide a direct experimental confirmation of our first-principles finding for their importance in limiting conductivity of these alloys. More generally, our calculations indicate that growth under maximally Te- and Se- poor conditions represents the ideal regime in which to realize maximally-resistive  $\text{Bi}_2\text{Te}_2\text{Se}$ , one of the most promising current candidates for use as a true topological insulator.

## Experimental Section

**First principles calculations:** density functional theory (DFT) calculations were performed using the projector augmented wave method<sup>[22]</sup> implemented within the VASP code.<sup>[23]</sup> Exchange and correlation were treated within the PBE functional,<sup>[24]</sup> using a planewave cutoff of 300 eV and a *k*-point sampling of  $10 \times 10 \times 10$  for the 5 atom tetradymite unit cell. The structure was deemed to be converged when the forces on all of the atoms were less than  $0.01 \text{ eV}\text{\AA}^{-1}$ . Defect calculations were performed using the method described in Ref. [27], using  $4 \times 4 \times 1$  expansions of the hexagonal representation of the unit cell (i.e., 240 atom supercells) with a  $2 \times 2 \times 1$  Monkhorst-Pack special *k*-point grid. All calculations include spin-orbit coupling.

**Experimental details:**  $\text{Bi}_2\text{Se}_3$ ,  $\text{Bi}_2\text{Se}_2\text{Te}$ ,  $\text{Bi}_2\text{Te}_2\text{Se}$ , and  $\text{Bi}_2\text{Te}_{2.5}\text{Se}_{0.5}$  crystals were prepared by melting high purity elements (5N) of Bi, Se, and Te in the ratios 2:3:0, 2:2:1, 2:1.05:1.95, and 2:0.5:2.5,

respectively. ARPES measurements were performed using Scienta R4000 hemispherical analysers at beamline 5-4 of the Stanford Synchrotron Radiation Lightsource (SSRL) and the CASSIOPEE beamline of synchrotron SOLEIL. The photon energies were between 14 and 18 eV, and the sample temperature was  $\sim 10 \text{ K}$ . Samples were cleaved at the measurement temperature in a pressure better than  $3 \times 10^{-11} \text{ mbar}$ . Further theoretical and experimental details are given in supplementary information.

## Acknowledgements

D. O. S. is grateful to the Ramsay Memorial Trust and University College London for the provision of a Ramsay Fellowship. All calculations were made possible by the UK's HPC Materials Chemistry Consortium, which is funded by the EPSRC (grant no. EP/F067496). The experimental work was supported by the ERC, Scottish Funding Council, and the EPSRC. SSRL is supported by the US Department of Energy, Office of Basic Energy Sciences. We also acknowledge SOLEIL for provision of synchrotron radiation facilities and we would like to thank Patrick Le Fèvre and Amina Taleb-Ibrahimi for assistance in using beamline CASSIOPEE.

Received: January 13, 2012

Revised: February 24, 2012

Published online: March 19, 2012

- [1] H. Zhang, C.-X. Liu, X.-L. Qi, X. Dai, Z. Fang, S.-C. Zhang, *Nat. Phys.* **2009**, *5*, 438.
- [2] Y. Xia, D. Qian, D. Hsieh, L. Wray, A. Pal, H. Lin, A. Bansil, D. Grauer, Y. S. Hor, R. J. Cava, M. Z. Hasan, *Nat. Phys.* **2009**, *5*, 398.
- [3] Y. L. Chen, J. G. Analytis, J.-H. Chu, Z. K. Liu, S.-K. Mo, X. L. Qi, H. J. Zhang, D. H. Lu, X. Dai, Z. Fang, S. C. Zhang, I. R. Fisher, Z. Hussain, Z.-X. Shen, *Science*. **2009**, *325*, 178.
- [4] D. Hsieh, Y. Xia, D. Qian, L. Wray, J. H. Dil, F. Meier, J. Osterwalder, L. Pathey, J. G. Checkelsky, N. P. Ong, A. V. Federov, H. Lin, A. Bansil, D. Grauer, Y. S. Hor, R. J. Cava, M. Z. Hasan, *Nature*. **2009**, *460*, 1101.
- [5] M. Z. Hasan, C. L. Kane, *Rev. Mod. Phys.* **2010**, *82*, 3045.
- [6] J. G. Checkelsky, Y. S. Hor, R. J. Cava, N. P. Ong, *Phys. Rev. Lett.* **2011**, *106*, 196801.
- [7] C. B. Satterthwaite, R. W. Ure, *Phys. Rev.* **1957**, *108*, 1164.

- [8] G. Wang, X. G. Zhu, Y. Y. Sun, Y. Y. Li, T. Zhang, J. Wen, X. Chen, K. He, L. L. Wang, X. C. Ma, J. F. Jia, S.-B. Zhang, Q.-K. Xue, *Adv. Mater.* **2011**, *23*, 2929.
- [9] T. C. Harmann, B. Paris, S. E. Miller, H. L. Goering, *J. Phys. Chem. Solids.* **1957**, *2*, 181.
- [10] S.-B. Zhang, S.-H. Wei, A. Zunger, *J. Appl. Phys.* **1998**, *83*, 3192.
- [11] S.-B. Zhang, S.-H. Wei, A. Zunger, *Phys. Rev. Lett.* **2000**, *84*, 1232.
- [12] P. Y. Yu, M. Cardona, in *Fundamentals of Semiconductors 2<sup>nd</sup> Edition*, Springer-Verlag, Berlin Heidelberg, Germany **1999**.
- [13] P. D. C. King, T. D. Veal, P. H. Jefferson, J. Zuniga-Perez, V. Munoz-Sanjose, C. F. McConville, *Phys. Rev. B.* **2009**, *79*, 035203.
- [14] Z. Ren, A. A. Taskin, S. Sasaki, K. Segawa, Y. Ando, *Phys. Rev. B.* **2010**, *82*, 241306.
- [15] S.-Y. Xu, L. A. Wray, Y. Xia, R. Shankar, A. Petersen, A. Fedorov, H. Lin, A. Bansil, Y. S. Hor, D. Grauer, R. J. Cava, M. Z. Hasan, *arXiv* **2010**, *1007:5111*.
- [16] A very recent result has also shown that alloying Bi<sub>2</sub>Te<sub>3</sub> with Sb<sub>2</sub>Te<sub>3</sub> is similarly effective at tuning the chemical potential into the bulk bandgap.<sup>[17]</sup>
- [17] J. Zhang, C.-Z. Chang, Z. Zhang, J. Wen, X. Feng, K. Li, M. Liu, K. He, L. Wang, X. Chen, Q. K. Xue, X. Ma, Y. Wang, *Nat. Commun.* **2011**, *2*, 574.
- [18] Via deliberate *n*-type doping of the surface by impurity adsorption,<sup>[4,19]</sup> we confirmed that the bottom of the bulk conduction band in Bi<sub>2</sub>Te<sub>2</sub>Se is located approximately 0.15 eV above the Fermi level for the measurement shown in Figure 2(a).
- [19] P. D. C. King, R. C. Hatch, M. Bianchi, R. Ovsyannikov, C. Lupulescu, G. Landolt, B. Slomski, J. H. Dil, D. Guan, J. L. Mi, E. D. L. Rienks, J. Fink, A. Linblad, S. Svensson, S. Bao, G. Balakrishnan, B. B. Iversen, J. Osterwalder, W. Eberhardt, F. Baumberger, Ph. Hofmann, *Phys. Rev. Lett.* **2011**, *107*, 096802.
- [20] A. Walsh, Y. Yan, M. M. Al-Jassim, S.-H. Wei, *J. Phys. Chem. C* **2008**, *125*, 12044.
- [21] C. Persson, Y.-J. Zhao, S. Lany, A. Zunger, *Phys. Rev. B* **2005**, *72*, 035211.
- [22] S. Jia, H. Ji, E. Climent-Pascual, M. K. Fuccillo, M. E. Charles, J. Xiong, N. P. Ong, R. J. Cava, *Phys. Rev. B* **2011**, *84*, 235206.
- [23] S. Nakajima, *J. Phys. Chem. Solids* **1963**, *24*, 479.
- [24] G. Kresse, D. Joubert, *Phys. Rev. B* **1999**, *59*, 1758.
- [25] G. Kresse, J. Furthmuller, *Phys. Rev. B* **1996**, *54*, 11169.
- [26] J. P. Perdew, K. Burke, M. Ernzerhof, *Phys. Rev. Lett.* **1996**, *77*, 3865.
- [27] M. Burbano, D. O. Scanlon, G. W. Watson, *J. Am. Chem. Soc.* **2011**, *133*, 15065.